Environmental Science and Pollution Research (2023) 30:62832–62846
https://doi.org/10.1007/s11356-023-26486-4

RESEARCH ARTICLE

Remarkable photocatalytic performances towards pollutant degradation under sunlight and enhanced electrochemical properties of TiO_2/polymer nanohybrids

Mariadhas Jarvin[1] · Daniel Rani Rosaline[2] · Thamizharasan Gopalakrishnan[3] · Maniveldoss Beaula Ruby Kamalam[1] · Edson Luiz Foletto[4] · Guilherme Luiz Dotto[4] · Savariroyan Stephen Rajkumar Inbanathan[1]

Received: 9 August 2022 / Accepted: 11 March 2023 / Published online: 22 March 2023

Abstract

In this work, TiO_2-based nanocomposites containing polyaniline (PANI), poly(1-naphthylamine) (PNA), and polyindole (PIN) were synthesized by effective and simple routes and posteriorly employed as photocatalysts and supercapacitors. Characterization techniques such as XRD, FTIR, FESEM, UV, and PL were employed to investigate the structural, morphological, and optical properties of materials. XRD analysis confirmed the successful formation of TiO_2 and TiO_2/polymer nanocomposites. PANI, PNA, and PIN polymers were well distributed on the surface of TiO_2 nanoparticles and were investigated/explored from the FESEM analysis. The visible light absorption and the recombination rate of photogenerated charge carriers were confirmed by the UV–Vis and PL analysis. The photocatalytic properties of the nanocomposites were investigated towards malachite green (MG) dye degradation under sunlight. The dye degradation efficiency followed the order TiO_2/PNA > TiO_2/PANI > TiO_2 > TiO_2/PIN. The higher efficiency of TiO_2/PNA can be associated with its smaller bandgap energy compared to the other materials. Electrochemical properties of materials were also examined by cyclic voltammetry and galvanostatic charge–discharge measurements using a three-electrode experiment setup in an aqueous electrolyte. TiO_2/PNA nanocomposite showed higher supercapacitor behavior compared to the other materials due to higher electrical conductivity of PNA and redox potential of TiO_2 (pseudocapacitance).

Keywords Green synthesis · TiO_2/polymer · Photocatalysis · Malachite green · Sunlight · Supercapacitor

Introduction

Due to the growth of population and industrialization, the need for pure water is very urgent one for human life. Inadequate disposal of wastewater from industries can cause pollution of pure drinking water, and its consumption can cause diarrhea and bacterial and viral infections (Georgin et al. 2018; Salomón et al. 2021). At the same time, due to changes in human lifestyles and modern technology, people are very much interested in using various electronic portable devices with quick charging and long-lasting batteries. But the main problem is delay in charging time and the stability of the battery. So, the researchers and scientists are continuously researching to overcome all these problems by using nanomaterials and nanosized instruments. Nanoscience and nanotechnology are currently growing fields of science (Ahmed et al. 2014; Bayda et al. 2019; Hornyak and Rao 2016). In this way, nanosized metal oxides, such as ZnO, CuO, MgO, SnO_2, CdO, and TiO_2 have received

Responsible Editor: Philippe Garrigues

✉ Guilherme Luiz Dotto
guilherme_dotto@yahoo.com.br; guilherme.dotto@ufsm.br

Savariroyan Stephen Rajkumar Inbanathan
stephenrajkumarinbanathan@americancollege.edu.in

1 Post Graduate and Research Department of Physics, The American College, Madurai 625002, Tamil Nadu, India

2 Post Graduate and Research Department of Chemistry, Lady Doak College, Madurai 625002, Tamil Nadu, India

3 Department of Physics, School of Advanced Sciences, Vellore Institute of Technology, Vellore 632014, India

4 Chemical Engineering Department, Federal University of Santa Maria, Santa Maria 97105-900, Brazil

considerable attention, especially, TiO_2, due to its tremendous properties like light absorption capacity in the range of UV region and pseudocapacitive nature with redox states. There are different methods to synthesize TiO_2 nanoparticles (NPs), such as hydrothermal (Steinfeld et al. 2015), co-precipitation (Tripathi et al. 2014), sol–gel (Dubey et al. 2019), microwave (Jena et al. 2010; Singh and Nakate 2013), and sonochemical (Alammar et al. 2010; Arami et al. 2007). The previously mentioned methods can produce some undesirable substances during the synthesis process. In order to avoid this problem, green synthesis route can be employed, which constitutes an easy, cost-effective, and toxic-free procedure.

Green synthesis method does not need for any specific hazardous reducing agents. The green extract acts as a capping and reducing agents, which can be used for the synthesis of several materials. Depending on the reducing agent employed, certain properties of NPs were enhanced, such as morphology, porosity, and particle size. Several works addressing TiO_2 nanoparticle preparation by different green methods, such as fungi (Rajakumar et al. 2012), bacteria (Kirthi et al. 2011), enzymes (Biczak et al. 2014), and many plant extracts, like *Camellia sinensis* (Zhu et al. 2019), neem (Thakur et al. 2019), *Coriandrum* (Pushpamalini et al. 2021), *Ocimum basilicum* (Kantheti and Alapati 2018), and *Moringa oleifera* (Patidar and Jain 2017), have been addressed. Among the main existing forms of TiO_2, anatase is considered the more active. TiO_2 oxide has an indirect bandgap of 3.23 eV for anatase, while the rutile phase shows a direct bandgap of 3.06 eV and an indirect bandgap of 3.10 eV (Gupta et al. 2013; Sankapal et al. 2014). Due to its wide bandgap, it will be photoactive only under UV light. So, there is a need to improve the bandgap by doping with transition metals (Fe, Ni, Co, Mn, Bi) (Ali et al. 2017; Ganesh et al. 2012; Sarkar et al. 2013; Chauhan et al. 2012; Wang et al. 2016), noble metals (Pd, Pt, Au, Ag) (Wu et al. 2014; Hu et al. 2015; Armelao et al. 2007; Suwarnkar et al. 2014), non-metals (B, C, N, S) (Niu et al. 2020; Yang et al. 2015; Khan et al. 2021; Devi and Kavitha 2014), or conducting polymers (PIN, PNA, PANI, polypyrrole (PPY)) (Handore et al. 2017; Ameen et al. 2011; Yang et al. 2017; Ceretta et al. 2020; Leichtweis et al. 2021).

Electrically conducting polymers are fascinating materials due to their intrinsic properties, like high flexibility and stability. Poly (1-naphthylamine) (PNA) has a considerable small bandgap of 2.11 eV among the conducting polymers offered with electrochromic, environmentally stable, and strong visible light absorption. Due to its semiconducting property, it is used for applications like sensors and supercapacitors. However, there are few reports addressing the application of PNA as photocatalyst (Ameen et al. 2010; Riaz and Ashraf 2012). Another interesting two-dimensional conducting polymer is the polyaniline (PANI), whose bandgap range is 1.3–2.7 eV (Saha et al. 2020). Polyindole (PIN) is a wide bandgap semiconducting polymer (~4.4 eV). Redox potential for PIN is high compared to polypyrrole (PPY) and PANI, so it is feasible to be used for electrochemical studies (Mudila et al. 2019). PNA and PANI polymers are able to absorb visible light, and PIN exhibits absorption only at UV light. When the green-synthesized TiO_2 NPs are coupled with these polymers, the recombination rate is reduced, so it will enhance the photocatalytic activity. In addition, the high redox potential of these polymers makes them suitable for supercapacitor application.

In present, TiO_2 NPs were synthesized by a simple green method and posteriorly coupled on different conducting polymers, PNA, PANI, and PIN, to improve the electrochemical energy storage and catalytic activity. Photocatalytic degradation of organic dye and electrochemical performances of TiO_2 NPs, TiO_2/PANI, TiO_2/PNA, and TiO_2/PIN materials have been investigated using the methylene blue dye under sunlight and three-electrode cell setup. The TiO_2/PNA exhibits high catalytic efficiency as well as capacitive property compared to the other materials. To the best of our knowledge, this is the first to examine the TiO_2 with various conducting polymers for the two different applications, such as photocatalytic degradation of organic dye and supercapacitor.

Experimental section

Chemicals

For the synthesis of TiO_2, TiO_2/PANI, TiO_2/PNA, and TiO_2/PIN, green tea bags (*Camellia sinensis*) were used and purchased from a local market (Brooke Bond, Taj Mahal, India). Titanium (IV) isopropoxide ($C_{12}H_{28}O_4Ti$, 97%) was bought from Sigma-Aldrich. For the synthesis of TiO_2/PANI, aniline solution ($C_6H_5NH_2$, 97%, Merck) was used as a monomer, and ammonium persulfate (APS, $(NH_4)_2S_2O_8$, 99%, Merck) was used as an oxidizing agent. For the synthesis of TiO_2/PNA, 1-naphthylamine ($C_{10}H_9N$, 99%, Sigma-Aldrich) was used as a monomer, and APS was used as an oxidizing agent, in addition isopropyl alcohol ($(CH_3)_2CHOH$, 99%). Indole powder (C_8H_7N, 99%, Sigma-Aldrich) was used as a monomer for TiO_2/PIN synthesis, and anhydrous ferric chloride ($FeCl_3$, Merck) was employed as an oxidizing agent. Hydrochloric acid (HCl, 37%) and ethanol (C_2H_5OH) were obtained from Merck.

Preparation of tea extract

Ten grams of teabag (2 g × 5) was boiled in 200 mL of distilled water until the tea extract was extracted from the teabag. Then, the tea extract was cooled to room temperature and filtered using Whatman filter paper (pore size of 10 μm).

Finally, the obtained dark brown color solution of tea extract was stored in a dark bottle in the refrigerator for further use. Tea extract acts as a both reducing agent as well as a capping agent in TiO_2 NPs formation. It contains the metal potassium in the large amount of 92–151 mg L^{-1} and other metals, such as sodium (35–69 mg L^{-1}), calcium (1.9–3.5 mg L^{-1}), aluminum (1.0–2.2 mg L^{-1}), fluoride (0.8–2.0 mg L^{-1}), iron (0.020–0.128 mg L^{-1}), and manganese (0.52–1.9 mg L^{-1}). Tea extract also have an antioxidant polyphenol group. This phenolic group contains four flavonoid groups, like epigallocatechin gallate (EGCG) (117 to 442 mg L^{-1}), epicatechin (EC) (25 to 81 mg L^{-1}), epicatechin gallate (ECG) (203 to 471 mg L^{-1}), and epigallocatechin (EGC) (16.9 to 150 mg L^{-1}). In the first step, $C_{12}H_{28}O_4Ti$ is converted into Ti^0, and epigallocatechin (EGC) is used in the phenolic group. –OH is the major group in epigallocatechin (EGC) in the reduction process. The reduced TiOH particles are converted into TiO_2 NPs during the calcination process.

Green synthesis of TiO_2 nanoparticles

As prepared, 200 mL of tea extract was inserted into a conical flask and kept in the bath sonicator at the frequency of 40 kHz (50 W). At the same time, 5 mL of titanium (IV) isopropoxide was added dropwise into the tea extract solution, resulting in a pale brown color solution. After 12 h of continuous stirring at room temperature, the TiO_2 NPs were obtained. Then, the solids were cleaned by using ethanol and water until the impurities were removed by centrifugation. The colloidal supernatant was dried in the hot air oven at 60 °C for 4 h, and finally calcined for 300 °C for 4 h. The preparation route of TiO_2 NPs is shown in Fig. 1.

Preparation of TiO_2/PANI nanocomposite

The green-synthesized TiO_2 NPs (1 g) were added in 100 mL of 2 M HCl and sonicated for 1 h at room temperature. Then, 1 mL of aniline monomer was added into the previous solution and stirred for 30 min. After, 0.25 g of 10 mL ammonium persulfate was added dropwise into the TiO_2–aniline suspension under stirring condition. After maintenance under stirring at room temperature for 12 h, TiO_2/PANI suspension was obtained. The suspension was centrifuged and washed with ethanol and water and dried at 40 °C for 24 h. The TiO_2/PANI formation mechanism is illustrated in Fig. S1.

Preparation of TiO_2/PNA nanocomposite

The green-synthesized TiO_2 NPs (1 g) were added into 200 mL of distilled water and 40 mL of isopropyl alcohol and sonicated for 15 min at room temperature. Then, 0.1 g of 1-naphthylamine was mixed with ethanol (10 mL) and posteriorly inserted into the TiO_2 solution, under sonication, being stirred for 1 h. After, 0.1158 g of 10 mL APS was dropwise added on the TiO_2/monomer solution. Then, the mixture was stirred for 12 h at room temperature. The solution was centrifuged and washed with ethanol and water for several times. The colloidal supernatant was dried at 40 °C for 24 h. TiO_2/PNA nanocomposite was obtained according to the mechanism presented in Fig. S2.

Preparation of TiO_2/PIN nanocomposite

The green-synthesized TiO_2 NPs (1 g) were added in 200 mL of distilled water and sonicated for 20 min at room temperature. In other glass recipient, 1 g of indole monomer was mixed with ethanol (10 mL) under stirring and posteriorly added to TiO_2 solution, being kept under stirring for 45 min. After, 80 mL of $FeCl_3$ solution (0.1 M) was added to TiO_2-indole solution and maintained under stirred for 24 h at room temperature. The final solution was centrifuged and washed with ethanol and water for several times. The obtained solids were dried for 40 °C for 24 h. TiO_2/PIN nanocomposite was prepared according to the mechanism presented in Fig. S3.

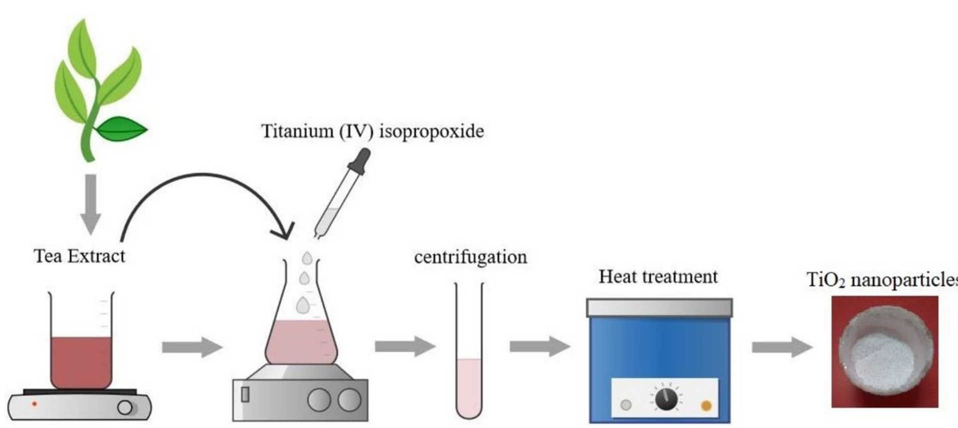

Fig. 1 Schematic representation of preparation route of TiO_2 NPs

Characterization techniques

The structural property of the samples was investigated by using an Ultima III Max diffractometer (Rigaku), with Cu-Ka ($\lambda = 1.5418$ Å) radiation at the operating condition of 40 keV and 30 mA. The diffraction pattern was recorded in the range 20–80° at grazing angle 1° and step size 0.01 deg. The functional groups and molecular structures of the samples were identified by a Fourier transform infrared spectrophotometer (Jasco FT/IR-4600), over the wavenumber range from 400 to 4000 cm^{-1}. The surface morphology and the presence of elements was investigated by field emission scanning electron microscopy (FESEM, SIGMA HV–Carl Zeiss), equipped with energy-dispersive X-ray spectroscopy (EDS, Bruker Quantax 200–Z10 EDS Detector). The optical behavior of the nanocomposites was investigated by a UV–Visible Jasco V-730 spectrophotometer. Room-temperature photoluminescence (PL) spectra of the nanocomposites were recorded by a Jasco spectrofluorometer (FP- 8300), at an excitation wavelength of 325 nm.

Photocatalytic assays

The photocatalytic dye degradation experiments were conducted for the TiO_2 NPs, TiO_2/PANI, TiO_2/PNA, and TiO_2/PIN materials, using malachite green (MG) dye as a model pollutant molecule. Dye concentration of 3 mg L^{-1}, pH of the solution = 7, and catalyst amount of 0.0125 g were employed for the photocatalytic degradation experiments. The experiments were conducted under sunlight on October 7–12, 2021, timing 10 am to 3 pm in Madurai (9.9759°N, 78.1393°E). Madurai City receives an incidence of global solar radiation around 5.0 kWh/m^2/day in the October month (Lakshmi et al. 2017). Before the photocatalytic experiment, the photocatalyst was added to MG aqueous solution (150 mL) and stirred (150 rpm) in the dark for 30 min to reach the adsorption equilibrium. Once the adsorption process was over, 5 mL of aliquots were collected and noted as “0” min. After that, the solution was left in the sunlight, and each 30 min, 5 mL of aliquots were collected, posteriorly centrifuged for 15 min, and characterized by a UV–Vis spectrophotometer (LI-295, 8W, 50 Hz), at a maximum wavelength of 620 nm. The degradation efficiency was calculated according to Eq. (1) (Ali et al. 2017; Jarvin et al. 2021).

$$\text{Degradation efficiency} = \frac{C_0 - C}{C_0} \times 100 \tag{1}$$

where C_0 and C are the solution concentrations at $t = 0$ and at an irradiation time *of t*, respectively.

Electrochemical measurements

A typical three-electrode system on an electrochemical analyzer (CHI-7007E) at room temperature was used to carry out the electrochemical measurements. The electrochemical cell was manufactured from Perspex glass. The outer surface was painted black, and the entire study was conducted inside the closed wooden box to prevent any impact of unwanted light on the working electrode. Platinum wire and Ag/AgCl were used as counter and reference electrodes in the Na_2SO_4 aqueous solution (0.1 M). The working electrode was prepared by a combination of nanocomposite material TiO_2 NPs, TiO_2/PANI, TiO_2/PNA, and TiO_2/PIN (90% weight), polyvinylidene difluoride (PVDF, 10% weight), and the appropriate amount of N-Methyl-2-pyrrolidone (10 mL). The paste-like 1 mg active material nanocomposite was loaded on 1 cm × 1 cm flexible graphite sheet dried at 80 °C for 12 h.

The specific capacitance C_{sp} (F/g) can be calculated from the cyclic voltammograms (CV), and galvanostatic charge-discharge (GCD), by the Eqs. (2) and (3) (Azman et al. 2018).

$$C_{sp} = \frac{\int IdV}{vm\Delta V} \tag{2}$$

$$C_{sp} = \frac{I\Delta t}{m\Delta V} \tag{3}$$

where I, t, V, ν, and m are the discharging current (A), discharging time (s), potential window (V), scan rate (mVs^{-1}), and mass of active material (g), respectively.

Results and discussion

Characterization results

Structural and crystalline properties of the synthesized nanocomposites were analyzed by X-ray diffraction technique, as shown in Fig. 2. Figure 2a exhibits the respective diffractograms for TiO_2, TiO_2/PANI, and TiO_2/PIN materials. TiO_2 NPs exhibit peaks located at 2θ values of 25.53, 37.88, 48.21, 54.07, 55.14, 62.84, 68.97, 70.43, and 75.18°, which corresponds to the planes of (101), (004), (200), (105), (211), (204), (220), (107), and (215), respectively. This result clearly shows the formation of TiO_2 NPs in anatase form. These results are associated with the JCPDS card No. 73–1764 (Maharana et al. 2021; Sofyan et al. 2018; Yang et al. 2012). TiO_2/PANI and TiO_2/PIN nanocomposites show similar patterns to the pristine TiO_2. TiO_2/PANI nanocomposite exhibits decreased peak intensity, and the position of the peak also

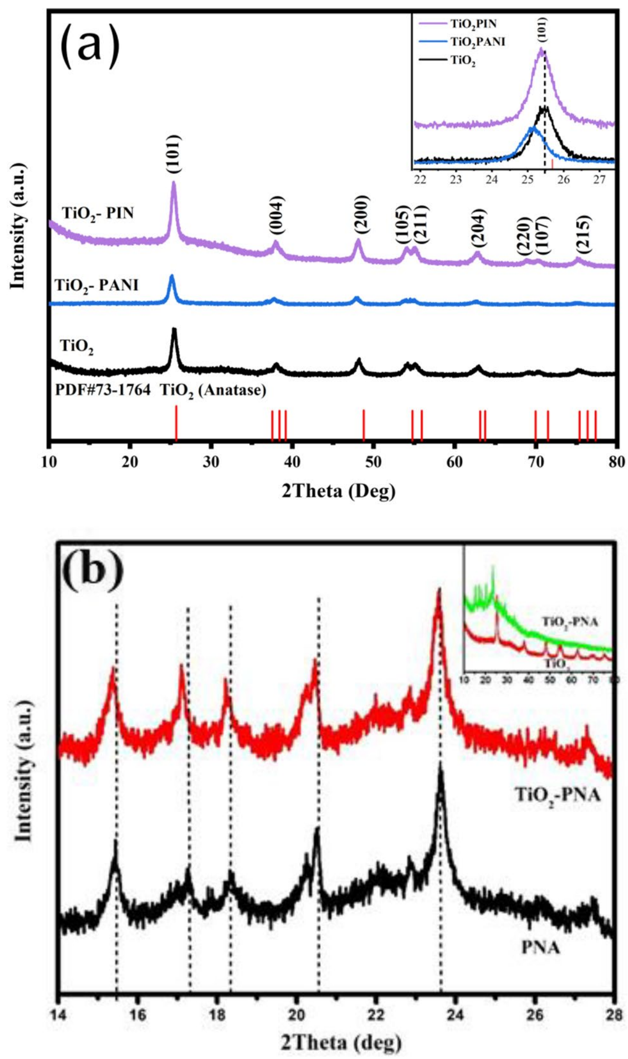

Fig. 2 XRD patterns of **a** TiO_2, TiO_2/PIN, and TiO_2/PANI and **b** PNA and TiO_2/PNA

shifts towards lower angle. This clearly shows that the incorporation of amorphous PANI to the TiO_2 NPs will alter the phase composition or crystallinity of the TiO_2 NPs (Wen et al. 2019; Sasikumar and Subiramaniyam 2018; Kumar and Pandey 2018). TiO_2/PIN nanocomposite also shows some changes in the intensity and width of the peak. This will make some changes in the crystallinity, but it will not create considerable changes in the TiO_2 NPs compared to TiO_2/PANI. The peaks at 25.53° and 48.21° reveal that the TiO_2/PIN nanocomposite is in anatase form [34]. Figure 2b shows the XRD patterns of PNA and TiO_2/PNA nanocomposite. In the case of TiO_2/PNA nanocomposite, it does not show any peaks related to the TiO_2, where only the peaks at 15.35, 17.24, 18.38, 20.51, and 23.66° were noticed, which are related to semi-crystalline nature of PNA (Ameen et al. 2010; Saidu et al. 2019; Riaz et al. 2016). This denotes that the insertion of PNA over TiO_2 NPs will increase the peak intensity of TiO_2/PNA nanocomposite, where a small shift towards lower angle was also noticed in the peak. This shows PNA deposited over the surface of TiO_2 NPs. This will be the most supporting parameter for photocatalytic activity. Table S1 shows the parameter comparison of the TiO_2, TiO_2/PNA and PNA samples.

The presence of functional groups in the synthesized samples was analyzed by the FTIR technique (Fig. 3). For TiO_2, the broad peak around 3320 cm^{-1} is due to the adsorbed water molecules on the material surface. The strong peak at 1730 cm^{-1} represents the carboxylic ester (-COOTi). Band at 1624 cm^{-1} denotes the water molecules absorbed on the TiO_2 NPs (Lu et al. 2015). Symmetric bending of CH_3 was confirmed by the appearance of a small peak around 1433 cm^{-1}. The peak at 1373 cm^{-1} clearly shows the presence of the carboxyl group. Transmittance peak within the range of 400–800 cm^{-1} shows the formation of Ti–O-Ti (Steinfeld et al. 2015; Thakur et al. 2019; Pushpamalini et al. 2021). TiO_2/PANI nanocomposite shows a similar IR spectrum to TiO_2, where only the peak at 1730 cm^{-1} decreased after polymerization. A small peak at 1128 cm^{-1} is due to the doped PANI's quinonoid group (Wen et al. 2019). Ti–O-Ti stretching mode of anatase peak is also present in TiO_2/PANI nanocomposite. This will suggest that TiO_2 does not alter or change during polymerization. For TiO_2/PNA nanocomposite, the peaks at 1390 cm^{-1} and 1604 cm^{-1} are due to the benzenoid (N-B-N) and quinonoid (N = Q = N) rings of PNA. The decreasing peaks at 1373 cm^{-1} and 1730 cm^{-1} indicate the interaction between TiO_2 and PNA. The existence of a peak at 711 cm^{-1} also confirms the polymerization of 1-naphthylamine monomer to PNA in the nanocomposite (Ameen et al. 2011). For TiO_2/PIN nanocomposite, the broad peak at the range of 3400 cm^{-1} denotes the –NH stretching of polyindole. The small transmittance peak at 1617 cm^{-1} indicates the aromatic C = C stretching. Band at 1445 cm^{-1} is assigned to the stretching of benzene on the indole ring. Band around 1333 cm^{-1} corresponds to the C = N stretching (Handore et al. 2017). The band at 744 cm^{-1} indicates that the benzene ring will not alter to any other form during the polymerization process.

Morphological properties and elemental composition of samples were analyzed by FESEM/EDS technique (Fig. 4). Figure 4a shows the FESEM image of TiO_2 oxide, presenting spherical and granular-shaped nanosized particles. The average particle size of 48 ± 23 nm was calculated using ImageJ software, represented by the histogram inset in Fig. 4b. TiO_2 NPs showed low agglomeration, which is due to the presence

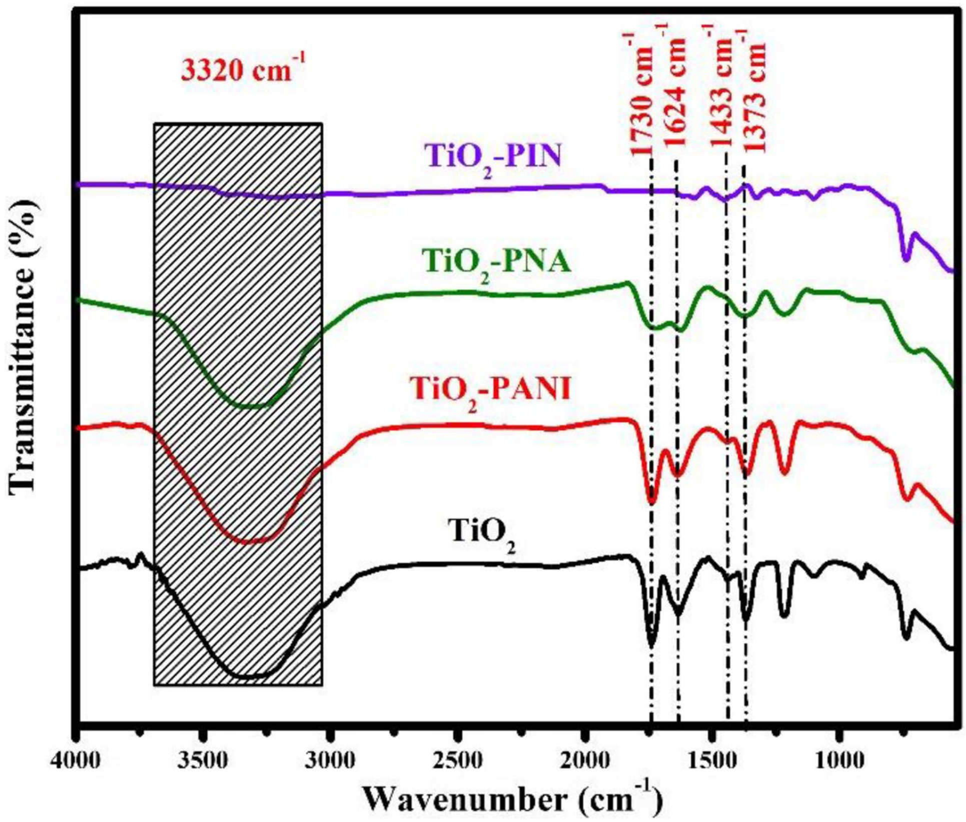

Fig. 3 FTIR spectra of TiO_2, TiO_2/PANI, TiO_2/PNA, and TiO_2/PIN

of biomolecules in the tea extract during the synthesis process. For TiO_2 NPs (Fig. 4b), the intense peaks at 4.6 keV and 5 keV and small intense peaks at 0.6 keV correspond to Ti, while the presence of O occurs at the range of 0.4 and 0.6 keV. The presence of oxygen vacancies leads to better photocatalytic application. The weight percentage of Ti was found the highest at 5.44%, and oxygen was 48.22%. The small peak of silicon (Si) (1.34%) corresponds to the optical reflection of Si surface during the characterization analysis. For TiO_2/PANI, the particles are more spherical, and their size also increased to 90 ± 70 nm, as shown in Fig. 4c. This occurred due to the coating of PANI over the surface of TiO_2 NPs. In addition, it is possible to observe that the particles are less agglomerated after doping with PANI. EDS spectrum of TiO_2/PANI composite is shown in Fig. 4d. The presence of peaks of Ti and O corresponds to the TiO_2 oxide, while S is attributed to the ammonium persulfate used during the synthesis process of the TiO_2/PANI composite. TiO_2/PNA shows an irregular shape, with a particle size of 65 ± 42 nm, as shown in Fig. 4e. This irregularity might arise due to the effective interaction between TiO_2 and PNA. Figure 4f shows the presence of Ti, O, S, and Cl elements, where trace residues of S and Cl elements are due to the compounds $FeCl_3$ and ammonium persulfate used in the synthesis process of the TiO_2/PNA nanocomposite. Figure 4g displays a porous structure with a particle size of 45 ± 20 nm, found for TiO_2/PIN nanocomposite. This porosity may be due to the high amount of PIN on the TiO_2/PIN composite. This structure is more feasible for supercapacitor applications. The presence of trace residue of Cl (Fig. 4h) is due to the $FeCl_3$ salt used during the synthesis process of the TiO_2/PIN composite.

The light absorption ability of TiO_2 and TiO_2/polymer composites was characterized by UV–Vis analysis, as shown in Fig. 5. Photocatalytic property greatly depends on the number of photons absorbed by the photocatalyst during the photocatalytic process. So, the optical absorption study is nut and bolt for photocatalytic material. The green synthesized TiO_2 shows a very sharp edge from 300 to 400 nm. This clearly shows that TiO_2 nanoparticles are more active in the UV region and absorb UV light only (Nabi et al. 2020). TiO_2/PANI nanocomposites' absorption peak shifted to a higher wavelength region compared to TiO_2 alone, which means that the material will absorb visible light. This is due to the well interaction between the PANI with TiO_2 nanoparticles (El-Hossary et al. 2020). The band around 400 nm is due to localized polarons, indicating protonated PANI (Mitra et al. 2019).

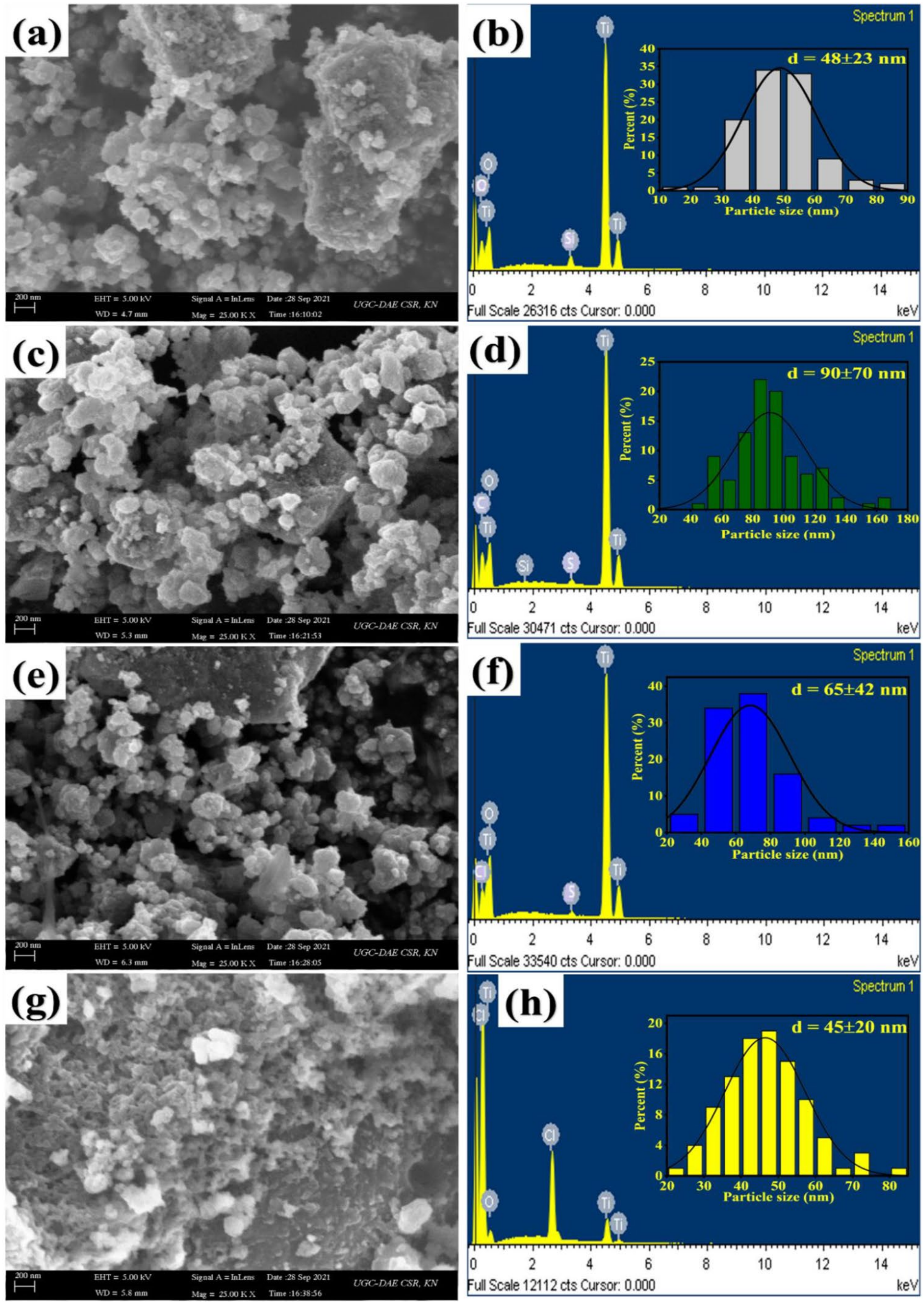

Fig. 4 FESEM images and EDS analysis for **a**, **b** TiO_2, **c**, **d** TiO_2/PANI, **e**, **f** TiO_2/PNA, and **g**, **h** TiO_2/PIN

For TiO_2/PNA, a very sharp edge around 300 nm occurs due to the combined effect of TiO_2 and π-π* transition in the benzenoid ring of PNA. The absorption peak at 513 nm can be due to the presence of excitonic and polaronic (*n*-π*) transitions of the quinonoid rings (Ameen et al. 2010; Riaz et al. 2008a, b; Riaz et al. 2008a, b). The absorption peak of TiO_2 is altered by the introduction of PNA (shifted to a higher wavelength region), and the peak intensity also increases. It clearly shows the interaction between TiO_2 and PNA moieties. The change in the intensity and the shift in the peaks occur due to the interaction of organic/inorganic composites through the hydrogen bond (Ameen et al. 2011, 2010). Similar to TiO_2/PNA, the TiO_2/PIN shows a shift in the peak, and the change in the intensity will confirm that the addition of PIN will change the TiO_2 property. The absorption peaks at 270 nm and 395 nm are due to the π-π* and n-π* transitions of PIN (Costa et al. 2012; Anjitha et al. 2019). The bandgap energy values

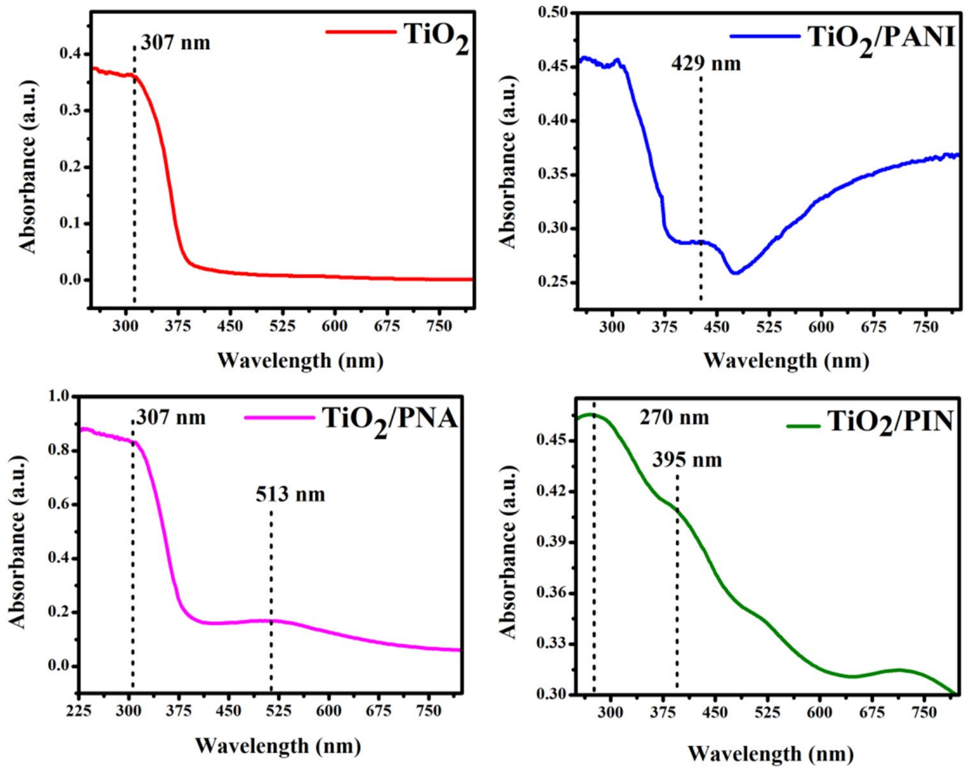

Fig. 5 UV–Visible spectra of TiO_2, TiO_2/PANI, TiO_2/PNA, and TiO_2/PIN

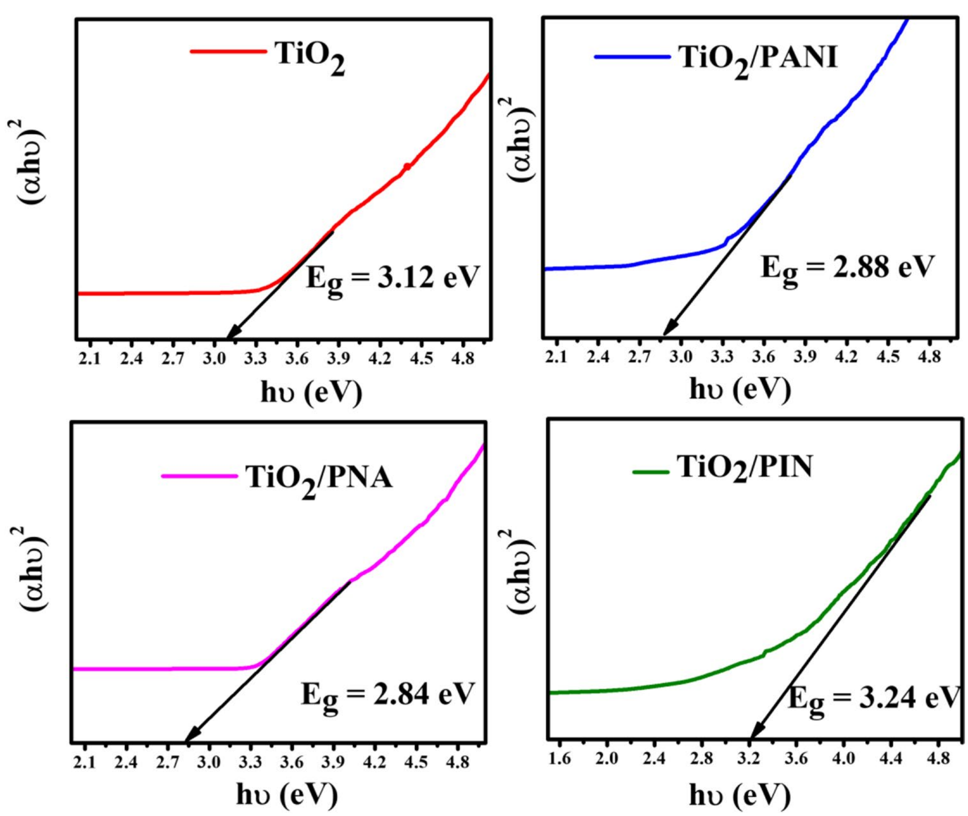

Fig. 6 Tauc plots of TiO_2, TiO_2/PANI, TiO_2/PNA, and TiO_2/PIN

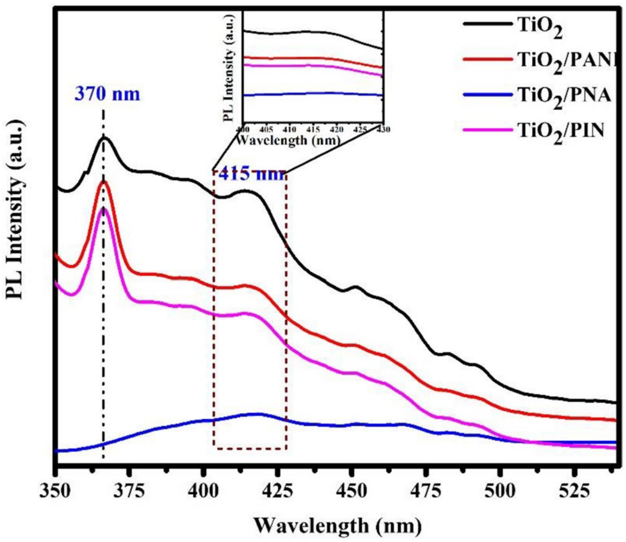

Fig. 7 PL spectra of TiO_2, TiO_2/PANI, TiO_2/PNA, and TiO_2/PIN

for TiO_2, TiO_2/PANI, TiO_2/PNA, and TiO_2/PIN were calculated using Tauc relation (El-Hossary et al. 2020), being 3.12 eV, 2.88 eV, 2.84 eV, and 3.24 eV, respectively, as shown in Fig. 6. Table S2 shows the crystallite size, particle size, and bandgap values of the TiO_2, TiO_2/PANI, TiO_2/PNA, and TiO_2/PIN samples.

Figure 7 exhibits the photoluminescence (PL) emission spectra of TiO_2 and TiO_2/polymer nanocomposites. Photoluminescence (PL) emission is a very useful analysis to study migration efficiency and recombination rate of electrons and holes. Photocatalytic activity always depends on the photoexcited electrons and holes, i.e., photocatalytic activity is proportional to the recombination rate of photoexcited electrons and holes and PL intensity (Ansari et al. 2014; Jing et al. 2014). The pure TiO_2 exhibits strong intensity peaks at 370 nm and 415 nm, while the TiO_2/PANI, TiO_2/PNA, and TiO_2/PIN nanocomposites show weak intensity peaks at the same wavelengths. It implies that there is a lower recombination rate of photoexcited electrons and holes in the hybrid nanocomposites than that the pure TiO_2. This will clarify that polymers could effectively interact with TiO_2 nanoparticles and effectively suppress the electrons and hole recombination.

Photocatalytic dye degradation activity

TiO_2 NPs and TiO_2/polymer composites show dye degradation efficiencies depending on their bandgap

Fig. 8 Dye photodegradation spectra for **a** TiO_2, **b** TiO_2/PANI, **c** TiO_2/PNA, and **d** TiO_2/PIN

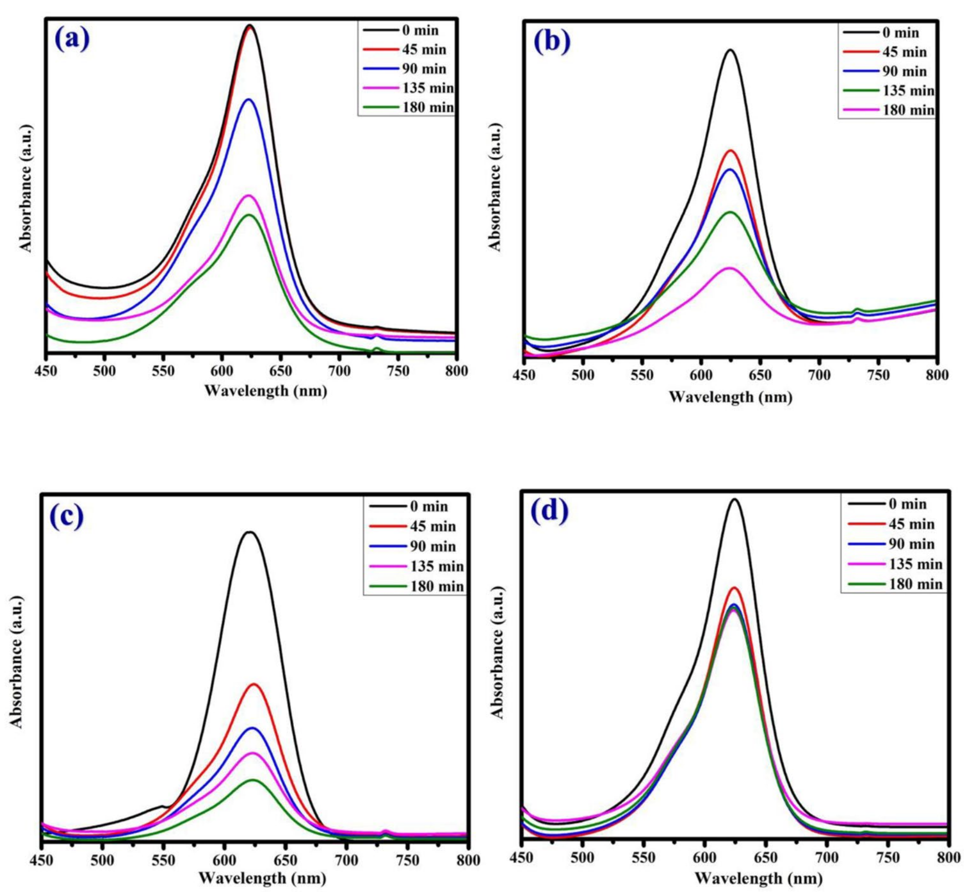

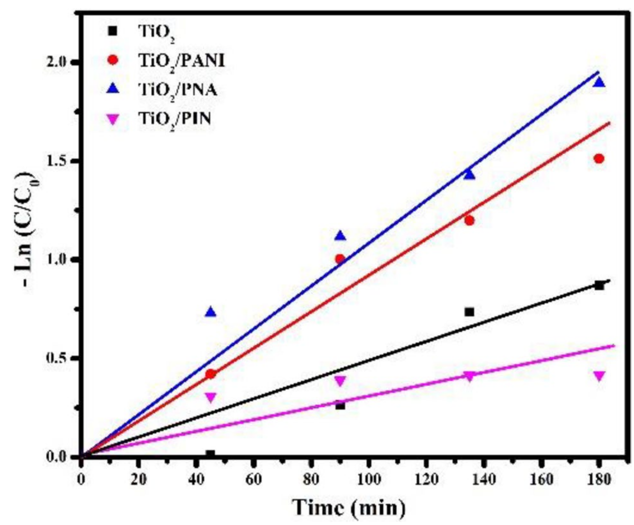

Fig. 9 Dye photodegradation kinetics for TiO_2, TiO_2/PANI, TiO_2/PNA, and TiO_2/PIN

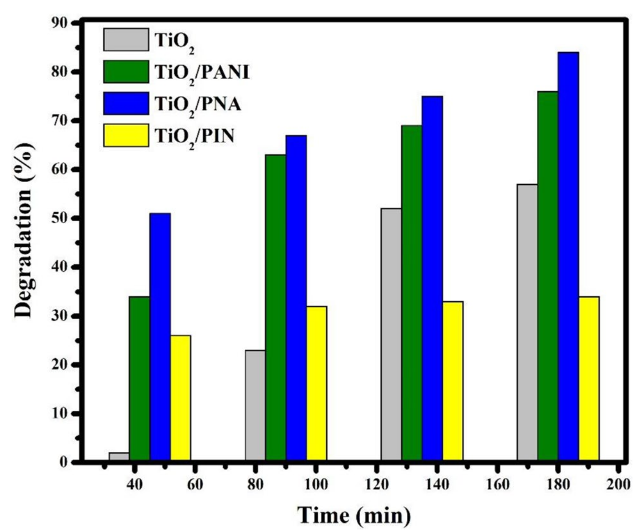

Fig. 10 Dye removal percentage using TiO_2 and TiO_2/polymer composites

values. Figure 8 shows the photocatalytic activities of TiO_2 NPs and TiO_2/polymer composites, while Fig. 9 shows the degradation efficiency and kinetic plots. TiO_2 NPs presented an efficiency of 57% in 180 min. The rate constant for MG photodegradation was estimated by linear regression, whose value found for TiO_2 NPs was 0.005 min^{-1} ($R^2 = 0.920$). For TiO_2/PANI and TiO_2/PNA composites, efficiencies of 76% and 84% within 180 min were observed, with photodegradation rate constants of 0.0085 min^{-1} ($R^2 = 0.9718$) and 0.01 min^{-1} ($R^2 = 0.9752$), respectively. TiO_2/PIN composite showed 34% efficiency in 180 min, with a rate constant of 0.0021 min^{-1} ($R^2 = 0.8562$). Figure 10 represents the dye removal percentage using TiO_2 NPs and TiO_2/polymer composites.

Photocatalytic degradation mechanism

Photodegradation activity of MG dye involves different stages of the process, including (i) interaction of MG dye with nanocomposite, (ii) photosensitization of nanocomposite, (iii) excitation of electrons (e −), (iv) transfer of e − to TiO_2 surface, and (v) degradation of MG dye into a colorless product. Under visible light irradiation, TiO_2 NPs does not excite the e − from the valence band (VB) to the conduction band (CB), because of its absorption in the UV absorption range. So, it will not act as a photosensitizer for TiO_2/polymer nanocomposites. PANI and PNA acted as good photosensitizers under visible light for TiO_2/PANI and TiO_2/PIN, due to their low bandgap energies, 1.8 eV and 2.1 eV, respectively. Insertion of polymers into the TiO_2 NPs makes the TiO_2/polymer composite a photosensitizer, as well as it will also hinder the e − and hole recombination process. Sunlight was absorbed by the polymers (PANI and PNA) and induced the transition of an electron to form the highest occupied molecular orbital (HOMO) to the lowest unoccupied molecular orbital (LUMO), i.e., π-π* transition (Saha et al. 2020). The conduction and valence band potentials of TiO_2 are − 0.3 eV and + 2.9 eV, and LUMO and HOMO values of PANI ranges from − 1 to -2 eV and 0.4 to 0.6 eV (Jahdi et al. 2020; Sakar et al. 2019; Ekande and Kumar 2021). The energy levels of TiO_2 and polymers are as follows: $E_{(LUMO)} > E_{(CB)} > E_{(HOMO)} > E(VB)$. This photogenerated e − is injected into the d-orbital (CB) of TiO_2. At the same time, holes in the valence band of TiO_2 are transferred to the highest occupied molecular orbit (HOMO) of the polymer, and oxidation process occurs. Holes will react with water to form •OH radicals. Then, the MG dye was degraded by the reactive oxygen species (ROS). A simplified general mechanism for the MG dye degradation is depicted as follows (Eqs. 4–11) (Amorim et al. 2021), as well as illustrated in Fig. 11.

$$\text{Polymer} + \text{hv} \longrightarrow \text{Polymer}\left(e^-_{CB} + h^+_{VB}\right) \tag{4}$$

$$\text{Polymer}(e^-) + TiO_2 \longrightarrow \text{Polymer} + TiO_2(e^-) \tag{5}$$

$$TiO_2(e^-) + O_2^- \longrightarrow TiO_2 + \cdot O_2^- \tag{6}$$

$$\cdot O_2^- + H^+ \longrightarrow HO_2 \tag{7}$$

$$HO_2 + \cdot O_2^- + H^+ \longrightarrow H_2O_2 + O_2 \tag{8}$$

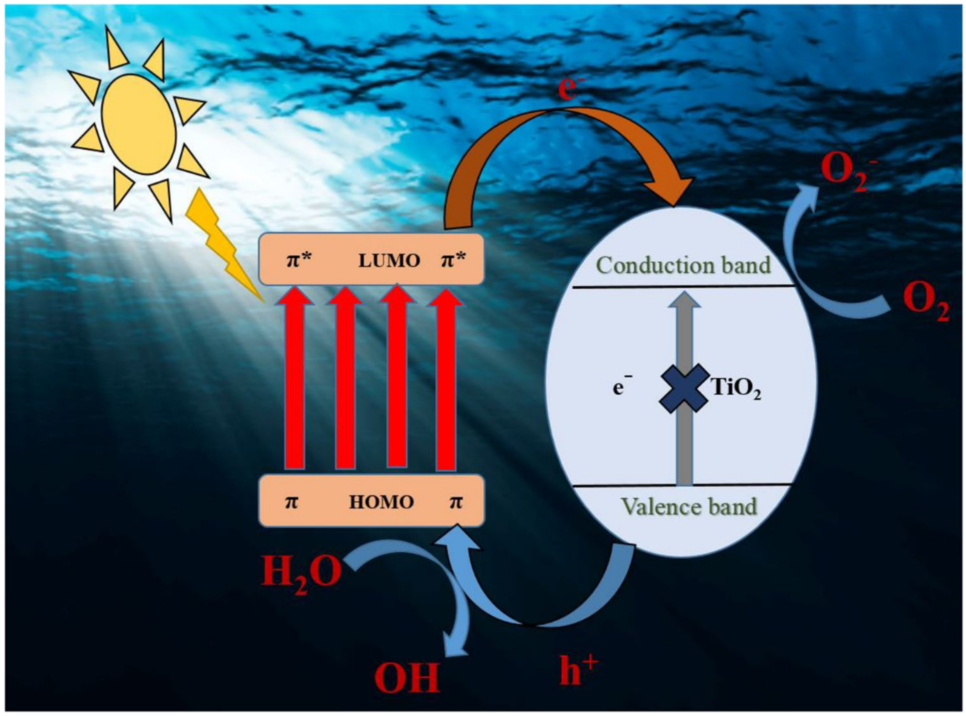

Fig. 11 The mechanism of MG dye photodegradation

$$H_2O_2 + e^- \longrightarrow OH^- + \cdot OH \tag{9}$$

$$\text{Polymer}\left(h^+\right) + H_2O \longrightarrow \cdot OH \tag{10}$$

$$\cdot OH + \text{MG Dye} \longrightarrow \textit{D}\text{egradation products}\ \left(CO_2, H_2O\right) \tag{11}$$

Electrochemical results

Electrochemical behaviors of the TiO_2 and TiO_2/polymer nanocomposites are illustrated in Fig. 12. The cyclic voltammograms (CV) were recorded from – 0.4 to 0.8 V at various scan rates (5 to 100 mV/s). For TiO_2 NPs, the CV curve shows a nearly rectangular shape, which reveals the reversible capacitive behavior of faraday redox reaction. All the CV curves of TiO_2 samples show the same profile under various scan rates from 5 to 100 mVs^{-1}. At the scan rate of 5 mVs^{-1}, TiO_2 NPs show a specific capacitance value of 69 Fg^{-1}. When increasing the scan rate to 100 mVs^{-1}, the integrated area of the CV curve increases and in turn results in a decrease in capacitance. High specific capacitance at a low scan rate is due to the slow intercalation and deintercalation process of ions with the electrode material. At the high scan rate, ions do not have sufficient time to migrate into the active sites of the electrode, leading to a decrease in the capacitance value. TiO_2/PANI, TiO_2/PNA, and TiO_2/PIN composites show capacitance values of 55, 98, and 25 Fg^{-1}, respectively. Generally, conducting polymers have high redox potential, and it will combine with TiO_2 metal oxide synergistic effect created between polymer and the metal oxide. These properties make TiO_2/PNA nanocomposite a perfect supercapacitive material, while the other two nanocomposites show low capacitance values. Low capacitance values for TiO_2/PANI and TiO_2/PIN nanocomposites, due to the excess amount of PANI and PIN in the composites, will restrict the insertion of ions into the electrode materials. Generally, polymer materials have low mechanical stability when the polymer is combined with TiO_2 NPs, and it will prevent the breakage of polymer structure during the charging and discharging process. The capacitive behavior of the TiO_2 and TiO_2/polymer nanocomposites was also confirmed by the investigation through the galvanostatic charge–discharge technique at the operating potential window between – 0.4 and 0.8 V, for the specific current from 0.5 to 100 A/g. For all the nanocomposites, the curves are not ideal; straight lines show the faradic behavior of nanocomposite. The maximum specific capacitance of TiO_2/PNA was 53 F/cm^2 at 1 A/g current density, being superior when compared to other samples, which is attributed to its high surface area and large number of active sites. Figure 13 depicts the specific capacitance values of TiO_2 and TiO_2/polymer nanocomposites from the cyclic voltammograms (CV) and galvanostatic charge–discharge (GCD).

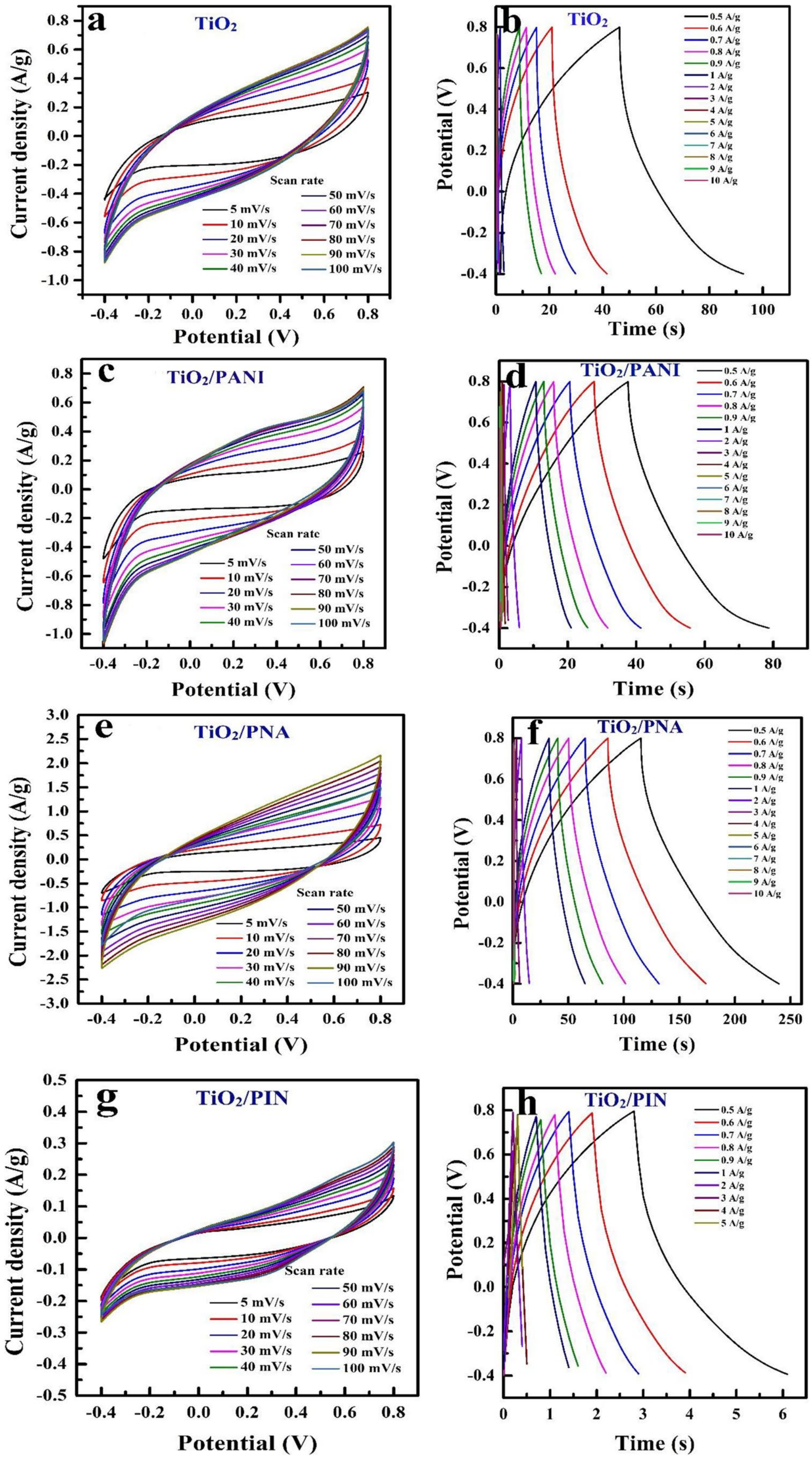

Fig. 12 **a**, **c**, **e**, **g** CV plots and **b**, **d**, **f**, **h** GCD plots of TiO_2, TiO_2/PANI, TiO_2/PNA, and TiO_2/PIN

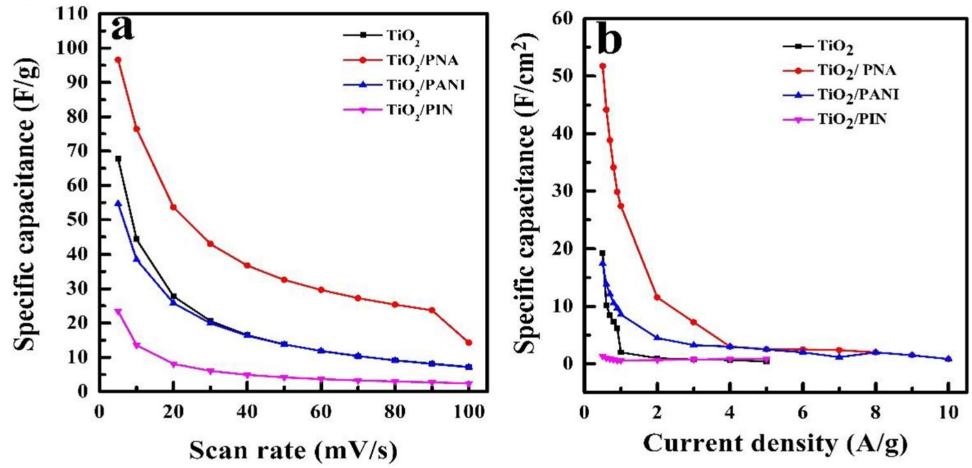

Fig. 13 Specific capacitance values from the **a** CV and **b** GCD at different scan rates and current densities

Conclusion

In this work, TiO_2/polymer hybrid materials were successfully prepared by an in situ chemical polymerization method. The TiO_2/PNA nanocomposite showed higher photocatalytic activity and capacitive behavior compared to the binary nanocomposites TiO_2/PANI, TiO_2/PIN, and pure TiO_2. The higher photocatalytic activity and better capacitive behavior occurred due to the insertion of PNA and PANI to the TiO_2. The extended visible light absorption and the higher charge separation enhanced the catalytic activity, and the conducting properties of the polymers increased the capacitive behavior. The low capacitive and catalytic behavior of TiO_2/PIN is due to the poor optical and electronic properties of the respective nanocomposite.

Supplementary Information The online version contains supplementary material available at https://doi.org/10.1007/s11356-023-26486-4.

Acknowledgements S.S.R. Inbanathan wishes to thank UGC-DAE-CSR, Indore Center (India). E.L. Foletto and G.L. Dotto would like to thank CNPq (National Council for Scientific and Technological Development, Brazil). The Brazilian authors would like to thank CAPES (Coordination for the Improvement of Higher Education Personnel) and CNPq (National Council for Scientific and Technological Development) for the financial support.

Author contribution Conceptualization, M. Jarvin; methodology, G. Thamizharasan, D. R. Rosaline; formal analysis and investigation, M. B. R. Kamalam, G. Thamizharasan, D. R. Rosaline; writing—original draft preparation, M. Jarvin, S. S. R. Inbanathan; writing—review and editing, G. L. Dotto, E. L. Foletto; funding acquisition, S. S. R. Inbanathan; supervision, S. S. R. Inbanathan. All authors read and approved the final manuscript.

Funding This work was supported by UGC-DAE Consortium for Scientific Research Indore Center grant Ref: CSR IC -236/2017–18/1317 (Dated: March 31, 2018).

Data availability The datasets used and/or analyzed during the current study are available from the corresponding author on reasonable request.

Declarations

Ethical approval Not applicable.

Consent to participate Not applicable.

Consent for publication Not applicable.

Competing interests The authors declare no competing interests.

References

Ahmed T, Imdad S, Yaldram K, Butt NM, Pervez A (2014) Emerging nanotechnology-based methods for water purification: a review. Desalin Water Treat 52:4089–4101

Alammar T, Birkner A, Shekhah O, Mudring AV (2010) Sonochemical preparation of TiO_2 nanoparticles in the ionic liquid 1-(3-hydroxypropyl)-3-methylimidazolium-bis (trifluoromethylsulfonyl) amide. Mater Chem Phys 120:109–113

Ali T, Tripathi P, Azam A, Raza W, Ahmed AS, Ahmed A, Muneer M (2017) Photocatalytic performance of Fe-doped TiO_2 nanoparticles under visible-light irradiation. Mater Res Expr 4:015022

Ameen S, Akhtar MS, Kim YS, Shin HS (2011) Nanocomposites of poly (1-naphthylamine)/SiO_2 and poly (1-naphthylamine)/TiO_2: comparative photocatalytic activity evaluation towards methylene blue dye. Appl Catal b: Environ 103:136–142

Ameen S, Akhtar MS, Kim YS, Yang OB, Shin HS (2010) Synthesis and characterization of novel poly(1-naphthylamine)/zinc oxide nanocomposites: application in catalytic degradation of methylene blue dye. Coll Polym Sci 288:1633–1638

Amorim SM, Steffen G, de Junior SJMN, Brusamarello CZ, Romio AP, Domenico MD (2021) Synthesis, characterization, and application of polypyrrole/TiO_2 composites in photocatalytic processes: a review. Polym Polym Compos 29:1055–1074

Anjitha T, Anilkumar T, Mathew G, Ramesan MT (2019) Zinc ferrite@polyindole nanocomposites: synthesis, characterization and gas sensing applications. Polym Compos 40:2802–2811

Ansari MO, Khan MM, Ansari SA, Lee J, Cho MH (2014) Enhanced thermoelectric behaviour and visible light activity of Ag@TiO_2/polyaniline nanocomposite synthesized by biogenic-chemical route. RSC Adv 4:23713–23719

Arami H, Mazloumi M, Khalifehzadeh R, Sadrnezhaad SK (2007) Sonochemical preparation of TiO_2 nanoparticles. Mater Lett 61:4559–4561

Armelao L, Barreca D, Bottaro G, Gasparotto A, Maccato C, Maragno C, Mahne D (2007) Photocatalytic and antibacterial activity of TiO_2 and Au/TiO_2 nanosystems. Nanotechnol 18:375709

Azman NHN, Nazir MS, Ngee LH, Sulaiman Y (2018) Graphene-based ternary composites for supercapacitors. Int J Energy Res 42:2104–2116

Bayda S, Adeel M, Tuccinardi T, Cordani M, Rizzolio F (2019) The history of nanoscience and nanotechnology: from chemical–physical applications to nanomedicine. Molecules 25:112

Biczak R, Pawłowska B, Bałczewski P, Rychter P (2014) The role of the anion in the toxicity of imidazolium ionic liquids. J Hazard Mater 274:181–190

Ceretta MB, Vieira Y, Wolskia EA, Foletto EL, Silvestri S (2020) Biological degradation coupled to photocatalysis by ZnO/polypyrrole composite for the treatment of real textile wastewater. J Water Proc Eng 35:101230

Chauhan R, Kumar A, Chaudhary RP (2012) Structural and photocatalytic studies of Mn doped TiO_2 nanoparticles. Spectrochim Acta A: Mol Biomol Spectrosc 98:256–264

Costa MBG, Juárez JM, Martínez ML, Cussa J, Anunziata AO (2012) Synthesis and characterization of a novel composite: polyindole included in nanostructured Al-MCM-41 material. Micropor Mesopor Mater 153:191–197

Devi LG, Kavitha RJMC (2014) Enhanced photocatalytic activity of sulfur doped TiO_2 for the decomposition of phenol: a new insight into the bulk and surface modification. Mater Chem Phys 143:1300–1308

Dubey RS, Krishnamurthy KV, Singh S (2019) Experimental studies of TiO_2 nanoparticles synthesized by sol-gel and solvothermal routes for DSSCs application. Res Phys 14:102390

Ekande OS, Kumar M (2021) Review on polyaniline as reductive photocatalyst for the construction of the visible light active heterojunction for the generation of reactive oxygen species. J Environ Chem Eng 9:105725

El-Hossary FM, Ghitas A, El-Rahman AM, Ebnalwaled AA, Shahat MA, Fawey MH (2020) Effect of UV-activated TiO_2 nanoparticles on the properties and performance of Pani-TiO_2 nanocomposite films for solar cell applications. IOP Conf Ser: Mater Sci Eng 956:012015

Ganesh I, Gupta AK, Kumar PP, Sekhar PSC, Radha K, Padmanabham G, Sundararajan G (2012) Preparation and characterization of Ni-doped TiO_2 materials for photocurrent and photocatalytic applications. Sci World J 2012:127326

Georgin J, Marques BS, Salla JS, Foletto EL, Allasia D, Dotto GL (2018) Removal of Procion Red dye from colored effluents using H_2SO_4-/HNO_3-treated avocado shells (Persea americana) as adsorbent. Environ Sci Poll Res 25:6429–6442

Gupta K, Singh RP, Pandey A, Pandey A (2013) Photocatalytic antibacterial performance of TiO_2 and Ag-doped TiO_2 against *S. aureus. P. aeruginosa* and *E. coli*. Beilstein J Nanotechnol 4:345–351

Handore K, Walunj D, Chhattise P, Chabukswar A, Mohite K, Dallavalle S, Chabukswar V (2017) Ultrasound synthesis of polyindole–TiO_2 nanocomposite and evaluation of antibacterial activity. Polym Plast Technol Eng 56:1259–1266

Hornyak GL, Rao AK (2016) Fundamentals of nanoscience and nanotechnology. In: Nanoscience in dermatology. Academic Press, pp 15–29. https://doi.org/10.1016/B978-0-12-802926-8.00002-1

Hu Y, Song X, Jiang S, Wei C (2015) Enhanced photocatalytic activity of Pt-doped TiO_2 for NO_x oxidation both under UV and visible light irradiation: a synergistic effect of lattice Pt^{4+} and surface PtO. Chem Eng J 274:102–112

Jahdi M, Mishra SB, Nxumalo EN, Mhlanga SD, Mishra AK (2020) Mechanistic pathways for the degradation of SMX drug and floatation of degraded products using F-Pt co-doped TiO_2 photocatalysts. RSC Adv 10:27662–27675

Jarvin M, Kumar SA, Vinodhkumar G, Manikandan E, Inbanathan SSR (2021) Enhanced photocatalytic performance of Hausmannite Mn_3O_4-rGO nanocomposite in degrading methylene blue. Mater Lett 305:130750

Jena A, Vinu R, Shivashankar SA, Madras G (2010) Microwave assisted synthesis of nanostructured titanium dioxide with high photocatalytic activity. Ind Eng Chem Res 49:9636–9643

Jing L, Yang ZY, Zhao YF, Zhang YX, Guo X, Yan YM, Sun KN (2014) Ternary polyaniline–graphene–TiO_2 hybrid with enhanced activity for visible-light photo-electrocatalytic water oxidation. J Mater Chem A 2:1068–1075

Kantheti P, Alapati P (2018) Green synthesis of TiO_2 nanoparticles using *Ocimum basilicum* extract and its characterization. Int J Chem Stud 6:670–674

Khan TT, Bari GAR, Kang HJ, Lee TG, Park JW, Hwang HJ, Jun YS (2021) Synthesis of N-doped TiO_2 for efficient photocatalytic degradation of atmospheric NOx. Catalysts 11:109

Kirthi AV, Rahuman AA, Rajakumar G, Marimuthu S, Santhoshkumar T, Jayaseelan C, Bagavan A (2011) Biosynthesis of titanium dioxide nanoparticles using bacterium Bacillus subtilis. Mater Lett 65:2745–2747

Kumar A, Pandey G (2018) Comparative photocatalytic degradation of rose bengal dye under visible light by TiO_2, TiO_2/PANI and TiO_2/PANI/GO nanocomposites. Int J Res Appl Sci Eng Technol 6:339–344

Lakshmi G, Gopinathan C, Deborrah SPM, Daniel T (2017) Estimation and prediction of global solar radiation at selected cities in Tamil Nadu, India. J Adv Phy Sci 1:13–17

Leichtweis J, Silvestri S, Vieira Y, Burgo TAL, Foletto EL (2021) A novel tin ferrite/polymer composite use in photo-Fenton reactions. Int J Environ Sci Technol 18:1537–1548

Lu K, He Q, Chen L, Ai B, Xiong J (2015) The comparative PDT experiment of the inactivation of HL60 on modified TiO_2 nanoparticles. J Nanomater 2015:540247

Maharana B, Ratha S, Shajahan AS, Chakraborty B, Jha R, Chatterjee S (2021) High charge-storage performance of morphologically modified anatase TiO_2: experimental and theoretical insight. Phys Rev Appl 15:034013

Mitra M, Ahamed ST, Ghosh A, Mondal A, Kargupta K, Ganguly S, Banerjee D (2019) Polyaniline/reduced graphene oxide composite-enhanced visible-light-driven photocatalytic activity for the degradation of organic dyes. ACS Omega 4:1623–1635

Mudila H, Prasher P, Kumar M, Kumar A, Zaidi MGH, Kumar A (2019) Critical analysis of polyindole and its composites in supercapacitor application. Mater Renew Sustain Energy 8:1–19

Nabi G, Raza W, Tahir MB (2020) Green synthesis of TiO_2 nanoparticle using cinnamon powder extract and the study of optical properties. J Inorg Organomet Polym Mater 30:1425–1429

Niu P, Wu G, Chen P, Zheng H, Cao Q, Jiang H (2020) Optimization of boron doped TiO_2 as an efficient visible light-driven photocatalyst for organic dye degradation with high reusability. Front Chem 8:172

Patidar V, Jain P (2017) Green synthesis of TiO_2 nanoparticle using Moringa oleifera leaf extract. Int Res J Eng Technol 4:1–4

Pushpamalini T, Keerthana M, Sangavi R, Nagaraj A, Kamaraj P (2021) Comparative analysis of green synthesis of TiO_2 nanoparticles using four different leaf extract. Mater Today: Proc 40:180–184

Rajakumar G, Rahuman AA, Roopan SM, Khanna VG, Elango G, Kamaraj C, Velayutham K (2012) Fungus-mediated biosynthesis and characterization of TiO_2 nanoparticles and their activity against pathogenic bacteria. Spectrochim Acta A: Mol Biomol Spectrosc 91:23–29

Riaz U, Ahmad S, Ashraf SM (2008a) Effect of dopant on the nanostructured morphology of poly (1-naphthylamine) synthesized by template free method. Nanoscale Res Lett 3:45–48

Riaz U, Ashraf SM, Budhiraja V, Aleem S, Kashyap J (2016) Comparative studies of the photocatalytic and microwave–assisted degradation of alizarin red using ZnO/poly(1-naphthylamine) nanohybrids. J Mol Liq 216:259–267

Riaz U, Ashraf SM (2012) Latent photocatalytic behavior of semiconducting poly(1-naphthylamine) nanotubes in the degradation of Comassie Brilliant Blue RG-250. Sep Purif Technol 95:97–102

Riaz U, Khan S, Islam MN, Ahmad S, Ashraf SM (2008b) Evaluation of antibacterial activity of nanostructured poly(1-naphthylamine) and its composites. J Biomater Sci Polym Ed 19:1535–1546

Saha S, Chaudhary N, Kumar A, Khanuja M (2020) Polymeric nanostructures for photocatalytic dye degradation: polyaniline for photocatalysis. SN Appl Sci 2:1–10

Saidu FK, Joseph A, Varghese EV, Thomas GV (2019) Characterization and electrochemical studies on poly (1-naphthylamine)-graphene oxide nanocomposites prepared by in situ chemical oxidative polymerization. J Solid State Electrochem 23:2897–2906

Salomón YLO, Georgin J, Franco DSP, Netto MS, Piccilli DGA, Foletto EL, Oliveira LFS, Dotto GL (2021) High-performance removal of 2,4-dichlorophenoxyacetic acid herbicide in water using activated carbon derived from Queen palm fruit endocarp (Syagrus romanzoffiana). J Environ Chem Eng 9:104911

Sankapal BR, Gajare HB, Dubal DP, Gore RB, Salunkhe RR, Ahn H (2014) Presenting highest supercapacitance for TiO_2/MWNTs nanocomposites: Novel method. Chem Eng J 247:103–110

Sarkar D, Mukherjee S, Chattopadhyay KK (2013) Synthesis, characterization and high natural sunlight photocatalytic performance of cobalt doped TiO_2 nanofibers. Phys E: Low-Dimens Syst Nanostruct 50:37–43

Sakar M, Prakash RM, Do TO (2019) Insights into the TiO_2-based photocatalytic systems and their mechanisms. Catalysts 9:680

Sasikumar M, Subiramaniyam NP (2018) Microstructure, electrical and humidity sensing properties of TiO_2/polyaniline nanocomposite films prepared by sol–gel spin coating technique. J Mater Sci: Mater Electron 29:7099–7106

Singh AK, Nakate UT (2013) Photocatalytic properties of microwave-synthesized TiO_2 and ZnO nanoparticles using malachite green dye. J Nanopart 2013:310809

Sofyan N, Ridhova A, Yuwono AH, Udhiarto A (2018) Preparation of anatase TiO_2 nanoparticles using low hydrothermal temperature for dye-sensitized solar cell. IOP Conf Ser: Mater Sci Eng 316:012055

Steinfeld B, Scott J, Vilander G, Marx L, Quirk M, Lindberg J, Koerner K (2015) The role of lean process improvement in implementation of evidence-based practices in behavioral health care. J Behav Health Serv Res 42:504–518

Suwarnkar MB, Dhabbe RS, Kadam AN, Garadkar KM (2014) Enhanced photocatalytic activity of Ag doped TiO_2 nanoparticles synthesized by a microwave assisted method. Ceram Int 40:5489–5496

Thakur BK, Kumar A, Kumar D (2019) Green synthesis of titanium dioxide nanoparticles using Azadirachta indica leaf extract and evaluation of their antibacterial activity. S Afr J Bot 124:223–227

Tripathi AK, Mathpal MC, Kumar P, Singh MK, Mishra SK, Srivastava RK, Agarwal A (2014) Synthesis based structural and optical behavior of anatase TiO_2 nanoparticles. Mater Sci Semicond Proc 23:136–143

Wang W, Zhu D, Shen Z, Peng J, Luo J, Liu X (2016) One-pot hydrothermal route to synthesize the Bi-doped anatase TiO_2 hollow thin sheets with prior facet exposed for enhanced visible-light-driven photocatalytic activity. Ind Eng Chem Res 55:6373–6383

Wen B, Waterhouse GI, Jia MY, Jiang XH, Zhang ZM, Yu LM (2019) The feasibility of polyaniline-TiO_2 coatings for photocathodic antifouling: antibacterial effect. Synth Met 257:116175

Wu RJ, Liu YS, Lai HF, Wang JH, Chavali M (2014) Promotion effect of Pd on TiO_2 for visible light photocatalytic degradation of gaseous formaldehyde. J Nanosci Nanotechnol 14:6792–6799

Yang C, Dong W, Cui G, Zhao Y, Shi X, Xia X, Wang W (2017) Enhanced photocatalytic activity of PANI/TiO_2 due to their photosensitization-synergetic effect. Electrochim Acta 247:486–495

Yang Y, Ni D, Yao Y, Zhong Y, Ma Y, Yao J (2015) High photocatalytic activity of carbon doped TiO_2 prepared by fast combustion of organic capping ligands. RSC Adv 5:93635–93643

Yang Z, Du G, Meng Q, Guo Z, Yu X, Chen Z, Zeng R (2012) Synthesis of uniform TiO_2@carbon composite nanofibers as anode for lithium ions batteries with enhanced electrochemical performance. J Mater Chem 22:5848–5854

Zhu X, Pathakoti K, Hwang HM (2019) Green synthesis of titanium dioxide and zinc oxide nanoparticles and their usage for antimicrobial applications and environmental remediation. In: Green synthesis, characterization and applications of nanoparticles. Micro Nano Technol, pp 223–263. https://doi.org/10.1016/B978-0-08-102579-6.00010-1

Publisher's note Springer Nature remains neutral with regard to jurisdictional claims in published maps and institutional affiliations.